Cell. Mol. Life Sci. (2016) 73:4121–4140
DOI 10.1007/s00018-016-2259-1

Cellular and Molecular Life Sciences

ORIGINAL ARTICLE

Hepatitis B virus inhibits insulin receptor signaling and impairs liver regeneration via intracellular retention of the insulin receptor

Sebastian Robert Barthel[1] · Regina Medvedev[1] · Thekla Heinrich[1] · Sarah Manon Büchner[1] · Nadja Kettern[1] · Eberhard Hildt[1,2]

Received: 18 December 2015 / Revised: 5 April 2016 / Accepted: 28 April 2016 / Published online: 7 May 2016

Abstract Hepatitis B virus (HBV) causes severe liver disease but the underlying mechanisms are incompletely understood. During chronic HBV infection, the liver is recurrently injured by immune cells in the quest for viral elimination. To compensate tissue injury, liver regeneration represents a vital process which requires proliferative insulin receptor signaling. This study aims to investigate the impact of HBV on liver regeneration and hepatic insulin receptor signaling. After carbon tetrachloride-induced liver injury, liver regeneration is delayed in HBV transgenic mice. These mice show diminished hepatocyte proliferation and increased expression of fibrosis markers. This is in accordance with a reduced activation of the insulin receptor although HBV induces expression of the insulin receptor via activation of NF-E2-related factor 2. This leads to increased intracellular amounts of insulin receptor in HBV expressing hepatocytes. However, intracellular retention of the receptor simultaneously reduces the amount of functional insulin receptors on the cell surface and thereby attenuates insulin binding in vitro and in vivo. Intracellular retention of the insulin receptor is caused by elevated amounts of α-taxilin, a free syntaxin binding protein, in HBV expressing hepatocytes preventing proper targeting of the insulin receptor to the cell surface. Consequently, functional analyses of insulin responsiveness revealed that HBV expressing hepatocytes are less sensitive to insulin stimulation leading to delayed liver regeneration. This study describes a novel pathomechanism that uncouples HBV expressing hepatocytes from proliferative signals and thereby impedes compensatory liver regeneration after liver injury.

Keywords α-Taxilin · HBV · Insulin resistance · Insulin receptor signaling · Liver disease · Nrf2

Abbreviations

HBV	Hepatitis B virus
HCC	Hepatocellular carcinoma
IR	Insulin receptor
ROI	Reactive oxygen intermediates
JNK	c-Jun N-terminal kinase
IRS	Insulin receptor substrate
Nrf2	NF-E2-related factor 2
NQO1	NAD(P)H-dependent quinone oxidoreductase 1
GPx	Glutathione peroxidase
GCLC	Glutamate-cysteine ligase catalytic subunit
γ-GCSc	γ-Glutamylcystein synthetase catalytic subunit
ARE	Antioxidant response element
Bim	Bcl-2-like protein
WT	Wild type
ALT	Alanin transaminase
AST	Aspartate transaminase
PEI	Polyethyleneimine
tBHQ	*tert*-Butylhydroquinone
PHH	Primary human hepatocytes
rtPCR	Real-time polymerase chain reaction
PCNA	Proliferating cell nuclear antigen
IGF-IR	Insulin-like growth factor 1 receptor
PDI	Protein disulfide isomerase
α-SMA	α-Smooth muscle actin
LHBs	Hepatitis B large surface protein

✉ Eberhard Hildt
eberhard.hildt@pei.de

[1] Department of Virology, Paul-Ehrlich-Institut, Langen, Germany

[2] German Center for Infection Research (DZIF), Gießen-Marburg-Langen, Gießen, Germany

SHBs	Hepatitis B small surface protein
CLSM	Confocal laser scanning microscope
FITC	Fluorescein isothiocyanate
SEM	Standard error of the mean
HE	Hematoxylin and eosin
HBsAg	Hepatitis B surface antigen
ER	Endoplasmic reticulum
galT	Galactosyltransferase
ESCRT	Endosomal sorting complexes required for transport
SNARE	Soluble *N*-ethylmaleimide-sensitive-factor attachment receptor
GCK	Glucokinase
GLUT4	Glucose transporter 4
HCV	Hepatitis C virus
HBx	Hepatitis B virus X
SOCS3	Suppressor of cytokine signaling 3

Introduction

Human hepatitis B virus (HBV) is a small enveloped, partially double-stranded DNA virus which belongs to the family of *Hepadnaviridae* [1]. Despite the existence of a prophylactic vaccine since the early 1980s, an estimate of 240 million individuals are chronically infected with HBV worldwide [2]. Currently, there is no curative treatment for chronic HBV infection and pathogenesis is incompletely understood [2]. Chronic HBV infection can cause liver fibrosis and ultimately results in cirrhosis [3]. Moreover, chronic hepatitis is the leading cause for the development of human hepatocellular carcinoma (HCC) accounting for more than 600,000 deaths annually [4, 5]. HBV-associated pathogenesis is considered to be mainly immune-mediated [6, 7]. However, chronic hepatitis can be characterized by a weak and inefficient T cell response which is unable to clear HBV from the liver [8]. An inefficient immune response to HBV sustains hepatocyte destruction and triggers excessive liver regeneration that can lead to fibrosis, cirrhosis and HCC [8]. Liver regeneration after injury is essential for liver tissue restoration [9]. Impairment of liver regeneration fosters fibrosis and development of liver diseases [10]. For the regulation of liver regeneration, insulin receptor signaling cascades play a pivotal role [11–14]. Patients with severe glucose intolerance or impaired insulin secretion even show high mortality following hepatectomy [15]. Insulin receptor (IR) signaling can be inactivated by elevated levels of reactive oxygen intermediates (ROI) which lead to activation of c-Jun N-terminal kinases (JNK) 1/2 and trigger Ser312-phosphorylation of the insulin receptor substrate (IRS) 1/2 [13]. A key player in defusing ROI and electrophiles is the cytoprotective transcription factor NF-E2-related factor 2 (Nrf2) which induces expression of ROI-detoxifying enzymes that prevent accumulation of ROI in the liver [16–18]. Examples are NAD(P)H quinone oxidoreductase (NQO1), glutathione peroxidase (GPx) or the catalytic subunit of the glutathione biosynthesis enzyme glutamate–cysteine ligase (GCLC) also known as γ-glutamylcysteine synthetase (γ-GCSc) [19]. NQO1 directly acts as a ROS scavenger catalyzing the reduction of reactive quinones to hydrochinones [20]. Expression of these enzymes is triggered by cis-acting antioxidant response elements (AREs) in the promoter of the corresponding genes [21]. Deficiency in Nrf2 causes inactivation of insulin receptor signaling and a delay in hepatocyte proliferation after partial hepatectomy due to increased intracellular levels of ROI, leading to JNK activation and subsequent Ser-phosphorylation of IRS1/2 [12, 13]. On the other hand, in transgenic mice that express constitutive active Nrf2 (caNrf2) liver regeneration is impaired due to delayed hepatocyte proliferation and enhanced apoptosis as expression of Bcl-2-like protein 11 (Bim) and the cyclin-dependent kinase inhibitor p15 is upregulated [22]. Interestingly, HBV directly activates Nrf2 and expression of Nrf2/ARE-regulated target genes [23]. This argues against an inhibitory effect of HBV on insulin signaling due to elevated ROI levels. Nevertheless, chronic HBV infection is associated with dysregulation of hepatocyte proliferation and retardation of liver regeneration [24]. However, the underlying mechanisms are not fully understood. Thus, the purpose of this study was to investigate liver regeneration and hepatic insulin receptor signaling in the context of HBV expression in vitro and in vivo. The present study demonstrates that in HBV transgenic mice liver regeneration after liver injury is impaired. Here, we propose a novel pathomechanism by which impairment of liver regeneration correlates with inhibition of proliferative insulin receptor signaling due to intracellular retention of the insulin receptor in HBV expressing cells.

Materials and methods

Mice

All mice used were on a C57Bl/6 background. The transgene in HBV transgenic mice consists of 1.3 copies of the complete HBV genome as described [25]. HBV transgenic Nrf2 homozygous knock-out mice were generated by crossing HBV transgenic mice with Nrf2 knock-out mice which were described previously [26]. Mice were treated intraperitoneally with a single dose (0.27 mL/kg body weight) of a 2 % solution of carbon tetrachloride (CCl_4) (Merck) in olive oil. At the respective days of post treatment

(1, 2, 3, 5 and 7 days), mice were narcotized by CO_2 inhalation and euthanized by cervical dislocation. For long-term treatment, wild type (WT) and HBV transgenic mice were treated over a period of 52 days with CCl_4 (0.17 mL/kg body weight) with a single CCl_4 injection (i.p.) per week. Mice were sacrificed and the liver was harvested 3 days after the last injection. Liver specimens were removed and fixed in 4 % formaldehyde (Carl Roth). Blood was obtained by cardiac puncture. Quantitative determination of alanine transferase (ALT), aspartate transaminase (AST) and glucose concentration in EDTA-serum of WT and HBV transgenic mice was determined using the Reflotron system (Roche) and the respective Reflotron based test strips (Roche). Primary mouse hepatocytes were isolated by retrograde two-step EGTA/collagenase (Sigma) perfusion as described [27]. All animal experiments were performed in accordance with institutional policies and had been approved by the local veterinary authorities of Darmstadt, Germany.

Cell culture and cell treatment

Human hepatoma-derived cell lines HepG2, Huh7.5, and stably HBV expressing cell lines HepAD38 [28] and HepG2.2.15 [29] were cultivated as described [28, 29]. Formation of the 3.5 kB transcript in HepAD38 cells was blocked by addition of tetracycline (1 µg/mL) to the medium. Cells were transiently transfected with plasmid DNA using linear polyethyleneimine (PEI) (Polysciences, Inc.) as described in [30] and were grown for 24 or 48 h. Cells were stimulated with *tert*-butylhydrochinone (tBHQ) (Sigma) for 8 h with 50 µM 24 h after transfection. Insulin (Roche) stimulation was performed with a concentration of 100 nM. Primary human hepatocytes (PHH) were isolated by modified two-step EGTA/collagenase perfusion procedure as described [31] and infected with HepAD38-derived supernatant as described [32].

Nrf2 knock-down

Cells were transfected with 40 nM Nrf2-specific (sc-37030) or control siRNA (sc-37007) (Santa Cruz Biotechnology) using a N-TER Nanoparticle siRNA Transfection System (Sigma) according to the manufacturer's protocol. 72 h after transfection cells were treated with 50 µM tBHQ for 16 h.

Plasmids

For HBV expression, a 1.2-fold HBV-genome ayw was used (pHBV1.2). Constitutively active (pcaNrf2) and transdominant negative Nrf2 expression constructs (ptdnNrf2) were described previously [33]. Plasmids encoding mCherry alone and N-terminally mCherry-tagged α-taxilin were kindly provided by Dr. Daniela Ploen. pUC19(–) and pEGFP-N1 (Clontech) served as control plasmids.

SDS-PAGE and western blot analysis

Proteins were separated by SDS-PAGE [34] and transferred onto methanol-pretreated Hybond-P PVDF membranes (Merck Millipore). The membrane was blocked using nonfat dry milk powder (Carl Roth). Antibody incubation was performed as described [35]. Protein bands were detected by exposition of the membrane to a scientific imaging film using a peroxidase substrate reagent (ECL) or the LI-COR Odyssee detection system (LI-COR). Equal loading was controlled by detection of β-actin.

Real-time PCR (rtPCR)

RNA isolation was performed using peqGOLD TriFast (PEQLAB) according to the manufacturer's instructions. For cDNA synthesis, 5 µg of total RNA were treated with DNase I (PEQLAB). First-strand synthesis was carried out using Random Hexamer Primer (Fermentas) and RevertAid H Minus M-MuLV Reverse Transcriptase (Fermentas). rtPCR was performed according to the manufacturer's instructions. Primers used for rtPCR are shown in Table 1.

Antibodies and ELISA

Polyclonal rabbit anti-IRβ (C-19, 1:300 for western blotting, 1:80 for immunofluorescence and immunohistochemistry), monoclonal mouse anti-NQO1 (A180, 1:300 for western blotting), polyclonal rabbit anti-γ-GCSc (H-300, 1:300 for western blotting), polyclonal rabbit anti-phospho-IRβ (Tyr1162/1163, 1:300 for western blotting), polyclonal rabbit anti-Txlna (H-66, 1:1000 for western blotting, 1:80 for immunohistochemistry), polyclonal rabbit anti-GAPDH (FL-335, 1:300 for western blotting), polyclonal rabbit anti-β-tubulin (H-235, 1:1000 for western blotting) and polyclonal rabbit anti-PCNA (FL-261, 1:100 for immunohistochemistry) antibodies were purchased from Santa Cruz Biotechnology. Polyclonal rabbit anti-IGF-I receptor β (IGF-IRβ, 1:300 for western blotting) was purchased from Cell Signaling Technology, monoclonal mouse anti-PDI (1:250 for western blotting) and monoclonal mouse anti-Calnexin (1:1000 for western blotting) from BD Transduction Laboratories. Polyclonal rabbit anti-NQO1 (1:80 for immunohistochemistry) from Abnova, the monoclonal mouse α-SMA-specific antibody was obtained from eBioscience (1:100 for immunohistochemistry). Monoclonal mouse anti-LHBs antibody Ma18/07 [36] (1:600 for western blotting) was kindly provided by Dr. Glebe, Gießen, Germany. Mouse monoclonal anti-HBV core (MAB16990) (1:400 for western

Table 1 Sequences of rtPCR primers (5′ → 3′)

Primer	Sequence
HBV_3.5kb_fwd	ctccaagctgtgccttggg
HBV_3.5kb_rev	cccacccaggtagctagag
IR_fwd	gtggtgatggagctgatgg
IR_rev	accatgcagtttctcgctg
Txlna_fwd	atgaagaaccaagacaaaaaga
Txlna_rev	ctggctgctgccgggac
GCLC_fwd	cccatggaggtgcaattaac
GCLC_rev	tgcgataaactccctcatcc
GLUT4_fwd	cctacgtcttccttctatttg
GLUT4_rev	ctcatctggccctaaatactc
GCK_fwd	tggaccaagggcttcaaggc
GCK_rev	catgtagcaggcattgcagcc
GAPDH_fwd	gacccttcattgacctcaac
GAPDH_rev	tggactgtggtcatgagtcc
RPL27_fwd	aaagctgtcatcgtgaagaac
RPL27_rev	gctgctactttgcgggggtag

blotting) was obtained from Chemicon. Polyclonal goat anti-SHBs (1:100 for immunohistochemistry) was purchased from DAKO and monoclonal mouse anti-β-actin (1:10,000 for western blotting) from Sigma. Monoclonal mouse Anti-Na^+/K^+-ATPase alpha (1:500 for western blotting) as well as ELISA kit for phospho-IRβ (Tyr1334) were purchased from Life Technologies. ELISA kit for detection of total IRβ was purchased from Cell Signaling Technology. Polyclonal goat Alexa Fluor 488-conjugated secondary antibodies (1:1000) were obtained from Invitrogen and polyclonal donkey Cy3-conjugated antibodies (1:400) were purchased from Jackson ImmunoResearch Laboratories for immunofluorescence and immunohistochemistry. For western blotting, polyclonal donkey secondary antibodies (1:5000) were obtained from LI-COR and polyclonal donkey peroxidase-conjugated secondary antibodies (1:2000) were purchased from GE Healthcare. ELISAs were performed according to the manufacturer's instructions.

Indirect immunofluorescence analysis

Indirect immunofluorescence analysis was performed as described previously [37]. Nuclei were counterstained with DAPI (Sigma). All experiments were performed on a confocal LSM (CLSM) 510 microscope (Zeiss) with a 40× EC Plan-Neo NA 1.3 oil objective (Zeiss) and a 100× alpha Plan-Apochromat NA 1.46 oil objective (Zeiss). DAPI fluorescence was excited using a 405 nm diode laser, Alexa488 fluorescence was excited using a 488 nm Argon laser and Cy3 fluorescence was excited using a 543 nm He–Ne laser, respectively. Images were acquired with the ZEN 2012 software (Zeiss). Experiments were performed at room temperature.

Fig. 1 Impaired liver regeneration and decreased insulin receptor activation in HBV transgenic mice after liver injury. **a** HE staining of representative liver sections (magnification ×100) of male wild type (WT) and HBV transgenic mice either untreated or at different time points after intraperitoneal injection of a single dose (0.27 mL/kg body weight) of CCl_4. Hepatic lesions are outlined in white dashed lines. Five animals per group were analyzed with comparable results. *Scale bar* represents 500 μm. **b** PCNA staining of liver sections (magnification ×200) derived from male WT and HBV transgenic mice 1, 2, 3, 5, and 7 days after CCl_4 treatment. *Scale bar* represents 50 μm. The graph represents the ratio of PCNA-positive nuclei and total nuclei (mean ± SEM) per visual field in male WT ($n = 3$) and HBV transgenic mice ($n = 3$ for day 1, day 5 and day 7, $n = 4$ for day 2 and day 3) after CCl_4 treatment. Three visual fields have been analyzed per animal. *n.d.* not detectable. $*p < 0.05$, $**p < 0.01$. **c** Quantification of tyrosine-phosphorylated insulin receptor β (pY [1334]-IRβ) by phospho-IRβ-specific ELISA 1, 2, 3, 5 and 7 days after CCl_4 treatment in liver lysates from male WT ($n = 5$ for day 1 and day 2, $n = 3$ for day 3, $n = 4$ for day 5 and day 7) and HBV transgenic mice ($n = 7$ for day 1, $n = 5$ for day 2, $n = 4$ for day 3, $n = 3$ for day 5 and day 7). The graph represents the ratio of pY-IRβ and the total amount of IRβ as determined by IRβ-specific ELISA (mean ± SEM). $*p < 0.05$, $**p < 0.01$. **d** ALT (*left graph*) and AST (*right graph*) activity was determined in the serum of untreated and CCl_4 long-term-treated WT and HBV transgenic mice (0.17 mL/kg body weight). The graphs represent the mean ± SEM from six long-term-treated animals in each group ($n = 6$). The serum of untreated mice (WT: $n = 2$; HBV: $n = 3$) served as control. $*p < 0.05$, $**p < 0.01$. **e** Paraffin-embedded liver sections of CCl_4 long-term-treated WT and HBV transgenic mice were deparaffinized, rehydrated and stained by Picro-sirius red. Representative images are shown in comparison to untreated animals (magnification ×100). The red color indicates collagenous fibers. Scale bar represents 500 μm. The amount of collagen was quantified by the intensity of the red color using ImageJ. The graph represents the mean ± SEM from untreated (WT: $n = 3$; HBV: $n = 4$) and long-term-treated WT ($n = 10$) and HBV transgenic ($n = 10$) mice. Five visual fields have been analyzed per animal. $*p < 0.05$. **f** Paraffin-embedded liver sections of CCl_4 long-term-treated WT and HBV transgenic mice were deparaffinized, rehydrated and stained for α-SMA using a mouse-derived primary antibody and a donkey-derived Cy3-coupled anti-mouse secondary antibody (*red* fluorescence). Nuclei was visualized by DAPI (*blue* fluorescence) (magnification ×200). *Scale bar* represents 100 μm. Representative images are shown in comparison to untreated animals. The amount of α-SMA was quantified by the intensity of the *red* color using ImageJ. The graph represents the mean ± SEM from untreated (WT: $n = 1$; HBV: $n = 1$) and long-term-treated WT ($n = 5$) and HBV transgenic ($n = 5$) mice. Five visual fields have been analyzed per animal. $**p \leq 0.01$

Immunohistochemistry analysis

Formalin-fixed and paraffin-embedded liver sections mounted on microscope slides were deparaffinized for 15 min in xylene and rehydrated for 10 min in 99 % ethanol, 10 min in 75 % ethanol and 5 min in ddH_2O. The slides were briefly boiled in 10 mM citrate buffer (pH 6) and incubated for 40 min. Slides were incubated for

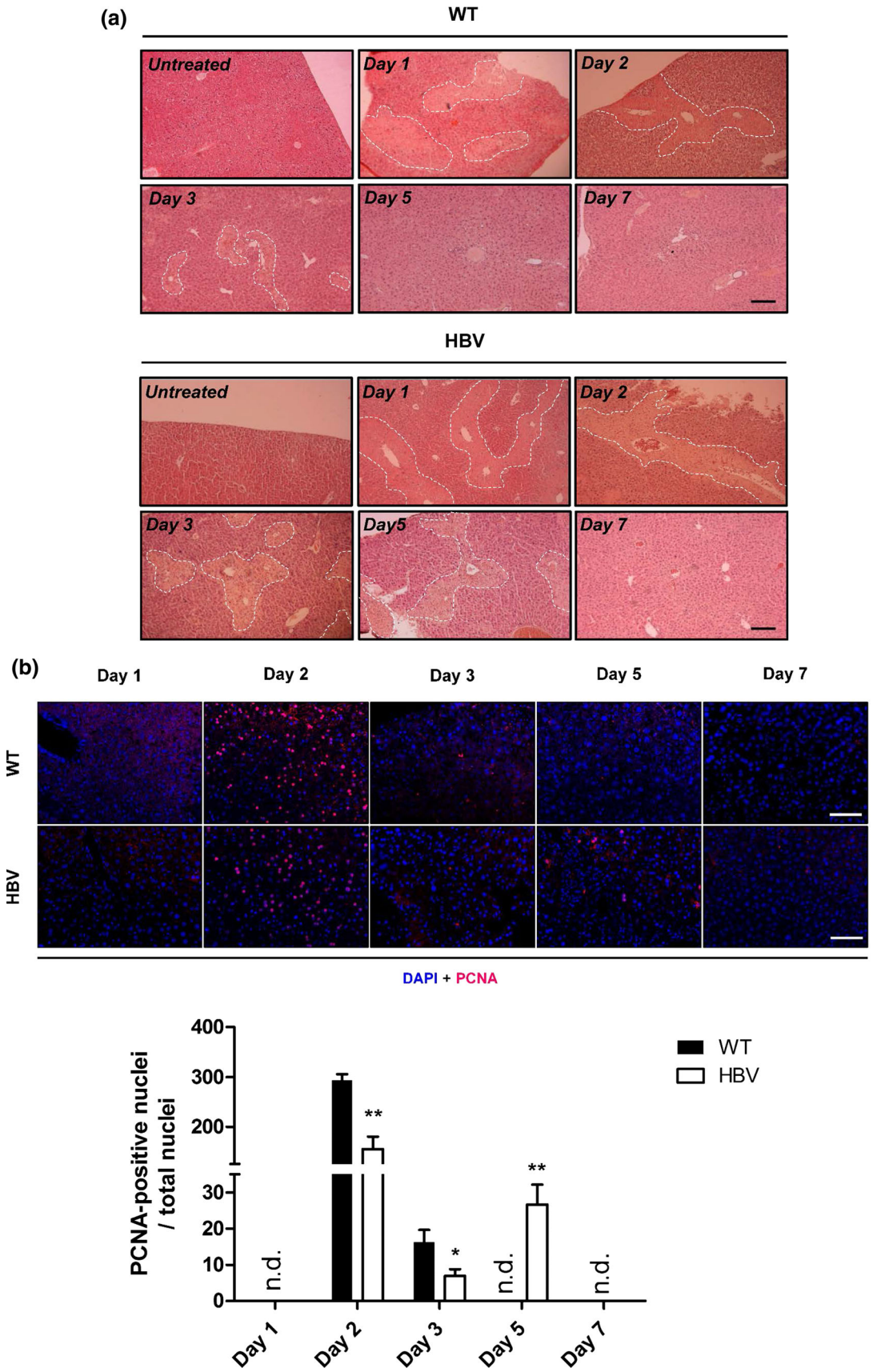
(a)
WT
Untreated
Day 1
Day 2
Day 3
Day 5
Day 7
HBV
Untreated
Day 1
Day 2
Day 3
Day5
Day 7
(b)
Day 1
Day 2
Day 3
Day 5
Day 7
WT
HBV
DAPI + PCNA
PCNA-positive nuclei / total nuclei
400
300
200
30
20
10
0
WT
HBV
**
*
**
n.d.
n.d.
n.d.
Day 1
Day 2
Day 3
Day 5
Day 7

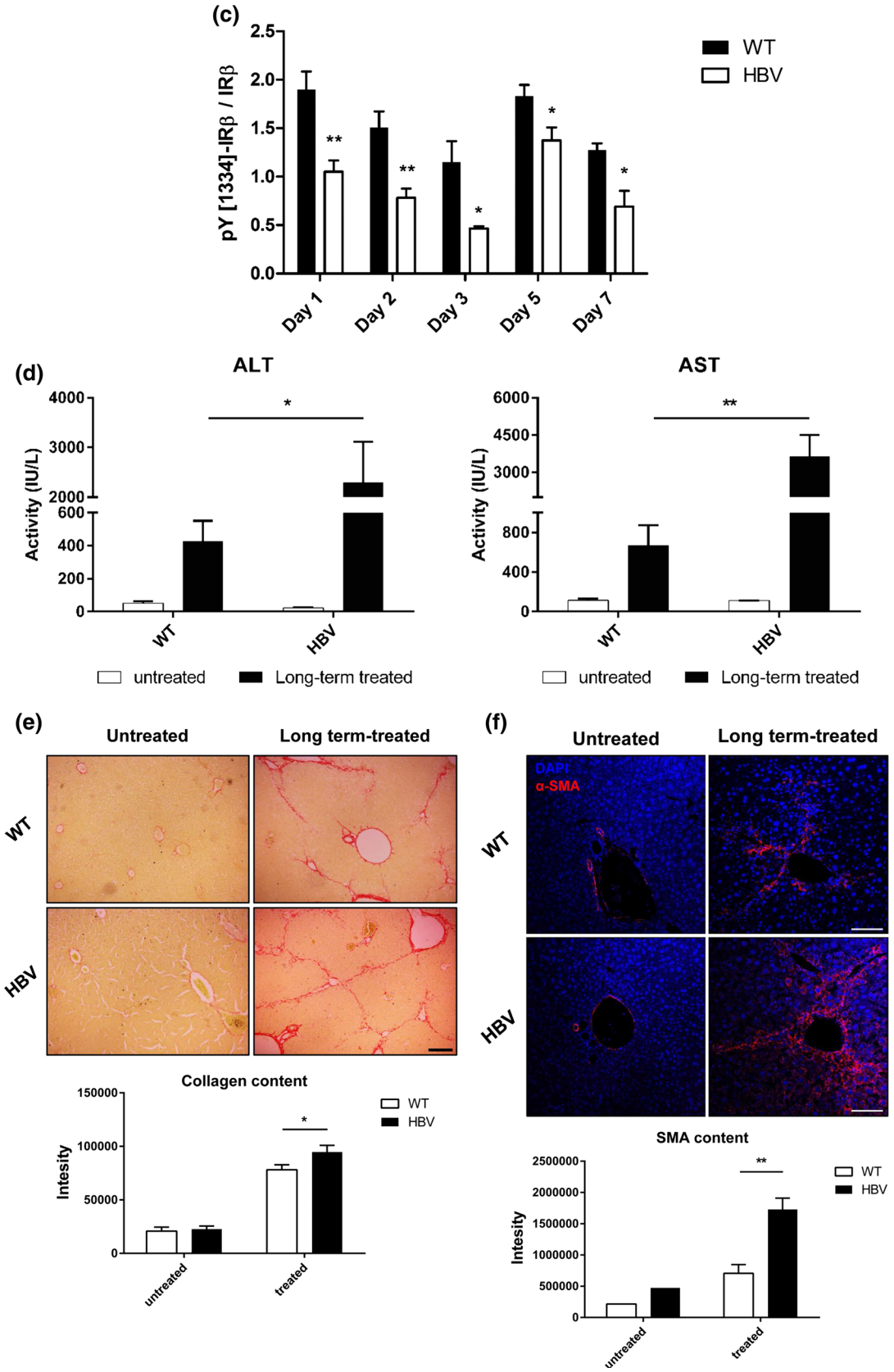

Fig. 1 continued

30–60 min with 10 % BSA in TBS buffer with 0.1 % Tween-20. Immunohistochemical staining was then performed as described using specific antibodies at room temperature in a humidified chamber [37]. Nuclei were counterstained with DAPI (Sigma). Liver sections were sealed with cover slips using Mowiol and analyzed on a LSM 510 microscope as described in the section above. Experiments were performed at room temperature. Picrosirius red staining using the dye Direct red 80 was performed for histological visualization of collagen type I and III fibers in liver sections and performed as described [38, 39].

FITC-insulin binding assay

Cells were seeded in a 96-well microplate. 24 h after seeding, DAPI (Sigma) was added to the medium (5 µg/µL) and cells were incubated for 30 min in the dark at room temperature. Cells were washed two times with ice-cold PBS and were then incubated with 4 µM of FITC-labeled insulin (Sigma) for 30 min in the dark at 4 °C. Cells were washed three times with ice-cold PBS and DAPI- ($\lambda_{ex} = 358$ nm, $\lambda_{em} = 461$ nm) and FITC- ($\lambda_{ex} = 488$ nm, $\lambda_{em} = 518$ nm) fluorescence was measured using a microplate reader (Tecan). FITC-fluorescence signal was normalized to the DAPI fluorescence signal.

Plasma membrane enrichment

Plasma membrane fragments were enriched by centrifugation according to [40].

Subcellular fractionation

Cells were cultured to confluency on 10 cm dishes. The medium was removed and cells were washed once with PBS. To each plate 1 mL of homogenization buffer (0.25 M sucrose, 1 mM EDTA, 10 mM HEPES-NaOH, pH 7.4), supplemented with a protease inhibitor, mixture was added and cells were scraped off. Cells were disrupted by 15–20 passages through a 26-gauge needle. Nuclei and unbroken cells were pelleted by centrifugation at $3000\times g$ for 10 min at 4 °C. The postnuclear supernatant was layered on top of a pre-formed 1–20 % iodixanol (OptiPrep™, Fresensius Kabi) linear gradient and centrifuged in a Beckman SW41Ti rotor (Beckman Coulter) at $200{,}000\times g$ for 3 h at 4 °C. Linear iodixanol gradients were prepared from a discontinuous gradient (1, 3, 5, 10, 15 and 20 % iodixanol in 0.25 M sucrose, 60 mM HEPES-NaOH, pH 7.4) by laying the tube 90° on the side for 1 h at room temperature. After centrifugation, fourteen fractions of 900 µL were collected from top to bottom. Fractions were analyzed by SDS-PAGE and western blotting.

Flow cytometry analysis

For flow cytometry analysis, cells were detached from cell culture dishes by accutase (Millipore) treatment for 15 min at 37 °C. For staining of the insulin receptor, cells were washed and resuspended in wash and staining buffer (PBS, 2 % BSA (AppliChem), 20 mM EDTA) and incubated with polyclonal rabbit anti-IRβ (1:100) for 30 min at room temperature. Cells were washed three times and then incubated with polyclonal goat Alexa Fluor 488-conjugated anti-rabbit antibody (1:500) for 30 min at room temperature in the dark. As control, cells were also incubated only with the secondary antibody without prior addition of anti-IRβ. Cells were fixed with 4 % formaldehyde in PBS for 10 min at room temperature, washed three times and were analyzed on a BD Accuri C6 flow cytometer (BD Biosciences). For FITC-insulin binding of mCherry and mCherry-α-taxilin-transfected cells 48 h post transfection, cells were detached by accutase treatment, resuspended in PBS and stained for 30 min at 4 °C in the dark with the fixable viability dye eFluor450 (eBiosciences) according to the manufacturer's instructions. After staining, cells were washed and incubated with 100 nM FITC-insulin (Sigma) for 30 min at 4 °C in the dark. Cells were fixed with 4 % formaldehyde in PBS for 10 min on ice and were analyzed on a LSRII SORP flow cytometer (BD Biosciences).

Galactosyltransferase activity assay

To determine galactosyltransferase activity after subcellular fractionation, a pH-sensitive assay based on the absorbance shift of phenol red was employed [41] and adapted to a 96-well format.

Statistical analysis

Experiments were performed on at least $n = 3$ independent experiments, unless otherwise indicated. Results are described as mean ± SEM. $^{*}p < 0.05$, $^{**}p < 0.01$. The significance of results was analyzed by ratio t test and two-tailed unpaired t test using GraphPad Prism version 5.04 for Windows, http://www.graphpad.com.

Results

Impaired liver regeneration in HBV transgenic mice

Chronic HBV infection is characterized by an equilibrium between destruction of hepatocytes and regeneration [8]. To study the impact of HBV on liver regeneration, CCl_4-induced liver damage was used as a model system. In HBV

transgenic mice and the corresponding WT mice as control, liver injury was analyzed at different time points (days 1, 2, 3, 5, and 7) after CCl_4 application by hematoxylin and eosin (HE) staining of liver samples. HE staining reveals more pronounced liver damage in HBV transgenic mice (Fig. 1a). The damage is mainly characterized by necrotic lesions as well as a substantial amount of apoptotic nuclei as determined by TUNEL assay (not shown). Lesions most prominently emanate from the blood vessels where CCl_4 enters the tissue via the bloodstream and damages the surrounding hepatocytes. In addition, while in WT mice after CCl_4-induced damage all lesions disappear within 5 days, in HBV transgenic mice liver regeneration is delayed and disappearance of the lesions is observed after 7 days at the earliest (Fig. 1a).

For a more detailed analysis of the regenerative process, expression of proliferating cell nuclear antigen (PCNA) in the nucleus of proliferating cells was analyzed by immunohistochemistry. While on 1 day after the initial CCl_4 treatment no PCNA-positive cells can be detected, proliferation peaks 2 days after liver damage, where the highest amount of PCNA-positive nuclei is readily detectable (Fig. 1b). Quantification of PCNA-positive nuclei 2 and 3 days after CCl_4-induced liver damage reveals a significant reduction in the amount of PCNA-positive nuclei in the liver of HBV transgenic mice as compared to the control mice (Fig. 1b). In addition, in contrast to WT mice, where 5 days after CCl_4 treatment liver regeneration is completed and no PCNA-positive cells can be observed, a significant amount of PCNA-positive nuclei is still detected in the liver of HBV transgenic mice. These data confirm that HBV transgenic mice reveal significantly reduced as well as delayed hepatocyte proliferation in accordance with the results from the HE staining.

Insulin receptor (IR)-dependent signaling represents a key factor controlling liver regeneration [12, 13]. In accordance with the decreased proliferation in HBV transgenic mice after CCl_4-induced liver damage, a reduced ratio of tyrosine-phosphorylated (pY-IRβ) to the total amount of IRβ was found during the course of 7 days after CCl_4-induced liver damage in the HBV transgenic mice as compared to the WT control mice (Fig. 1c). These data indicate a reduced activation of the insulin receptor signaling cascade in HBV transgenic mice compared to WT mice during the process of liver regeneration.

To investigate whether these markers of an impaired proliferative signaling indeed are reflected by an impaired regeneration leading to fibrosis, repetitive treatment with CCl_4 was performed over 52 days.

Analysis of ALT and AST levels as marker for liver damage in the serum after long-term liver injury reveals significant higher levels of the transaminases in the sera derived from HBV transgenic mice as compared to the control mice (Fig. 1d). Sirius Red staining for quantitative collagen determination and α-SMA staining by immunofluorescence microscopy of paraffin-embedded liver sections derived from WT and HBV transgenic mice reveal significant higher levels of collagen and α-SMA in the samples derived from HBV transgenic mice as compared to WT mice, reflecting that the onset of fibrotic processes in HBV transgenic mice is more pronounced (Fig. 1e, f).

Taken together, these data indicate that in HBV transgenic mice after CCl_4-dependently induced liver damage, liver injury is more pronounced and liver regeneration is decreased as compared to the WT controls.

Fig. 2 Increased levels of insulin receptor in HBV expressing cells. ▶ **a** Western blot analysis of cellular lysates derived from HepG2, HepAD38 and HepG2.2.15 cells using a rabbit-derived IRβ-specific antiserum. HBV surface antigen (HBsAg) was detected using a mouse-derived LHBs-specific antiserum (Ma18/07). Detection of β-actin served as loading control. **b** rtPCR of *IR*-specific transcripts in HepG2, HepAD38 and HepG2.2.15 cells ($n = 3$, mean ± SEM) referred to *GAPDH* as internal control. *IR* expression in HepG2 cells was set as 1. 3.5 kb HBV-specific transcripts were amplified using HBV-specific primers and were visualized by agarose gel electrophoresis as shown below the graph. $^{**}p < 0.01$. **c** Western blot analysis of cellular lysates derived from untreated HepG2 and HepAD38 cells and tetracyclin (Tet)-treated HepAD38 cells using a rabbit-derived IRβ-specific antiserum or a mouse-derived LHBs-specific antiserum. Detection of β-actin or β-tubulin served as loading control. **d** CLSM analysis of transiently HBV-transfected HuH7.5 cells (magnification ×1000), liver sections derived from an HBV transgenic mouse (magnification ×400) (**e**) and a patient with chronic hepatitis B (magnification ×400) (**f**). HBV expressing cells were visualized using mouse-derived LHBs- (Ma18/07) or goat-derived SHBs-specific antisera. For detection of IRβ a rabbit-derived antibody was used. Nuclei was visualized by DAPI. *Scale bar* represents 20 μm

Elevated amount of IR in HBV expressing cells

IR-dependent signaling plays an essential role with respect to the control of liver regeneration [11–13]. To investigate whether a reduced amount of IR is causative for impaired liver regeneration, the effect of HBV on the expression of IR was analyzed. Western blot analysis of cellular lysates derived from two independent cell lines that stably express HBV (HepG2.2.15 and HepAD38) and from the corresponding HBV-negative HepG2 cell line surprisingly reveal an elevated level of IR in the HBV expressing cell lines (Fig. 2a). Quantification of IR-specific transcripts by rtPCR confirm this observation (Fig. 2b). As both stable cell lines were independently established and harbor different HBV integrates, it is not likely that the observed effects are due to the integration. To definitively exclude this, it is useful that HBV expression in HepAD38 can be

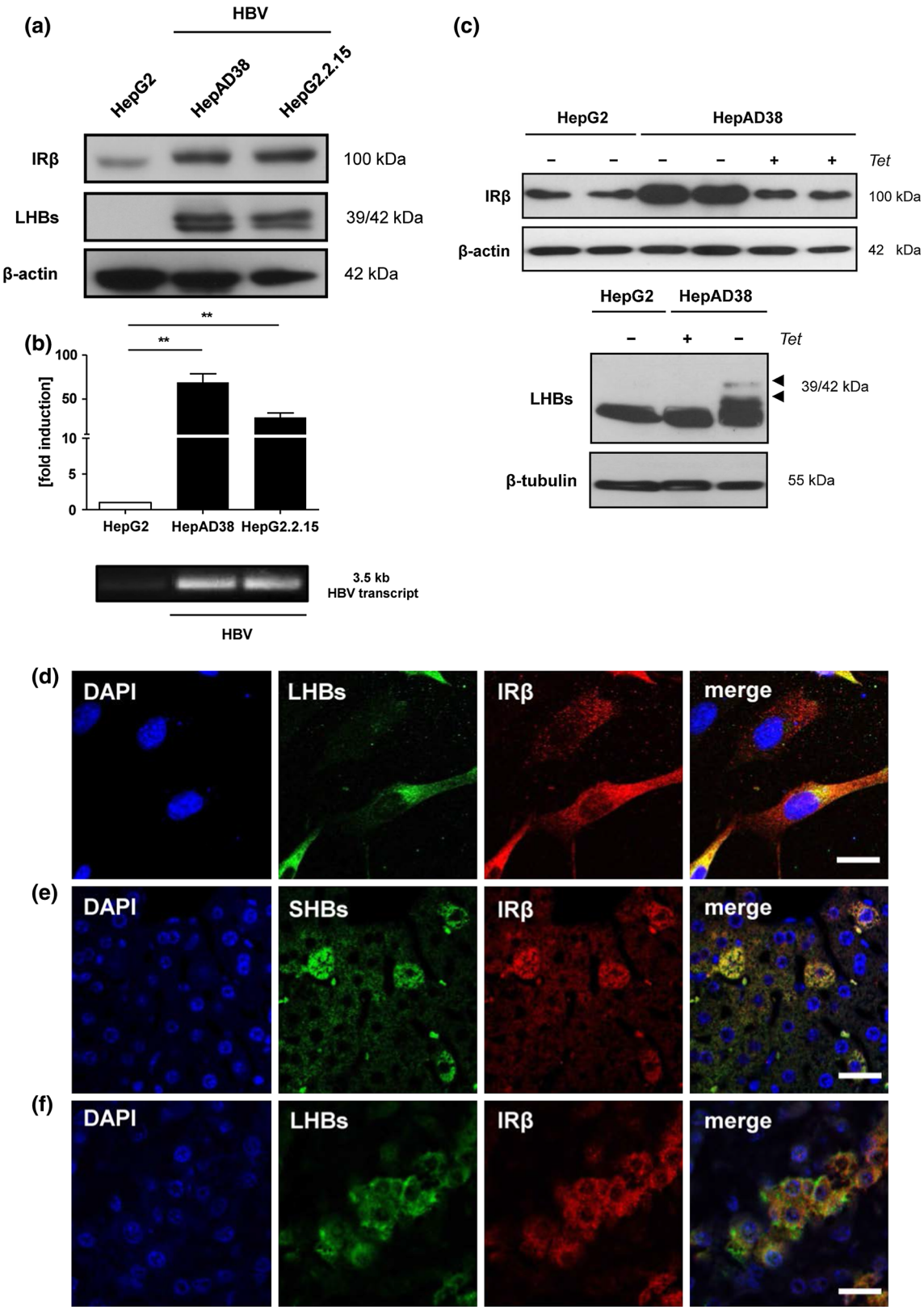
(a)
HBV
HepG2
HepAD38
HepG2.2.15
IRβ
100 kDa
LHBs
39/42 kDa
β-actin
42 kDa
(b)
**
**
[fold induction]
100
50
10
5
0
HepG2
HepAD38
HepG2.2.15
3.5 kb
HBV transcript
HBV
(c)
HepG2
HepAD38
– – – – + + Tet
IRβ
100 kDa
β-actin
42 kDa
HepG2
HepAD38
– + – Tet
LHBs
39/42 kDa
β-tubulin
55 kDa
(d)
DAPI
LHBs
IRβ
merge
(e)
DAPI
SHBs
IRβ
merge
(f)
DAPI
LHBs
IRβ
merge

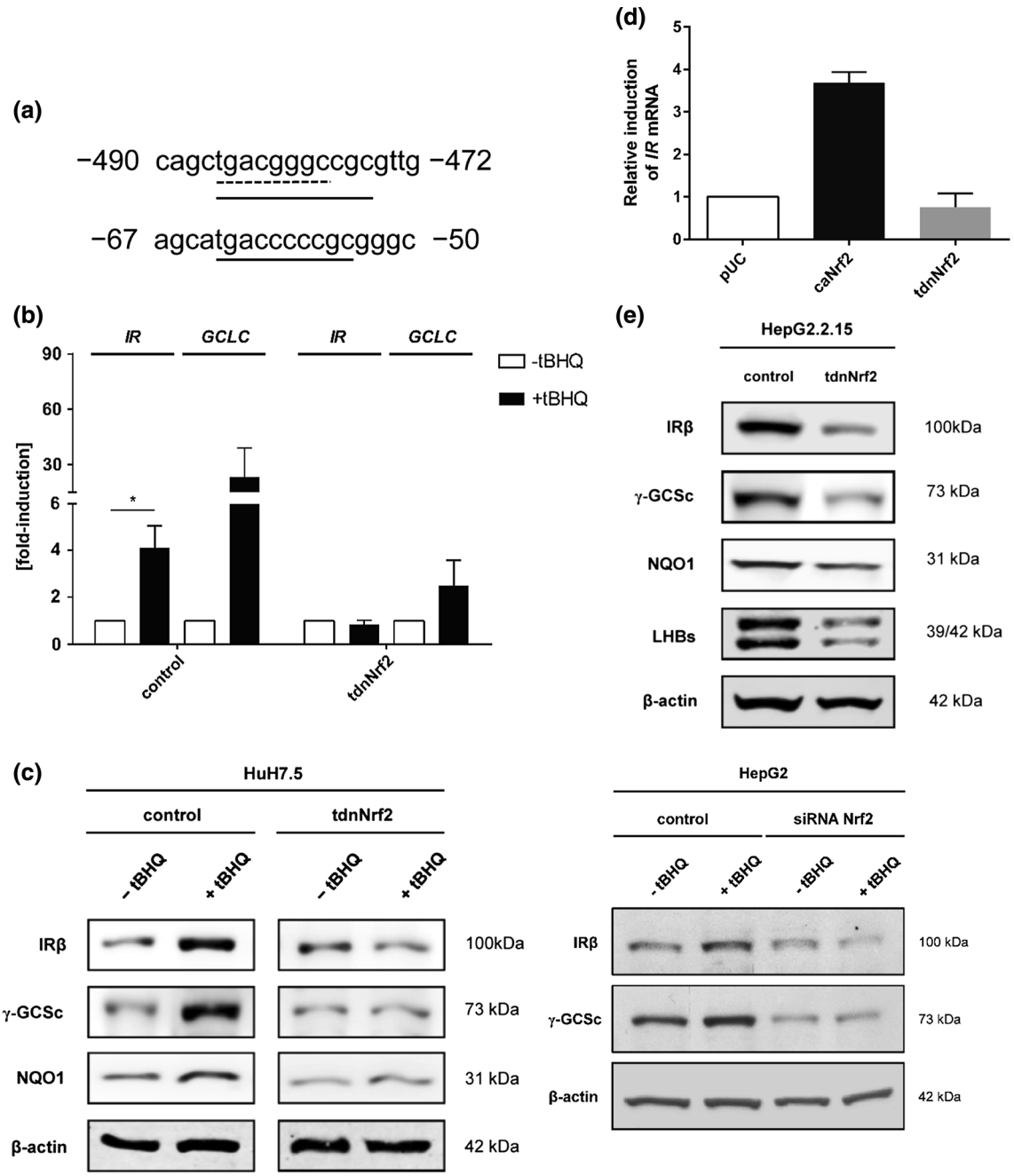

blocked by tetracycline (Fig. 2c). Indeed, Western blot analysis of lysates derived from HepAD38 cells grown in the presence of tetracycline show that the elevated levels of IR disappear (Fig. 2c). A level comparable to that found in HepG2 cells was observed. To further corroborate the observation that in HBV expressing cells the amount of IR is elevated, double immunofluorescence microscopy for detection of HBV surface antigen (HBsAg) and IR in Huh7.5 cells transiently transfected with a 1.2-fold HBV genome was performed (Fig. 2d). These experiments confirm that HBV expression is associated with an elevated amount of IR. Immunofluorescence microscopy of liver samples from HBV transgenic mice (Fig. 2e) or from patients suffering from chronic HBV infection (Fig. 2f) corroborate the observation that in HBV expressing cells a significantly elevated level of IR is found.

These data demonstrate that in vitro and in vivo HBV expression is associated with an elevated amount of IR.

◀**Fig. 3** Activation of Nrf2 induces insulin receptor expression. **a** Identification of putative ARE sequences (*underlined*) in the promoter region of the insulin receptor gene. The *dashed line* indicates a second, alternative ARE sequence. *Numbers* refer to the upstream position of the element within the promoter. **b** rtPCR of *IR*- and *GCLC*-specific transcripts in control (gfp) and transdominant negative Nrf2 (tdnNrf2) transfected HuH7.5 cells after treatment with tBHQ (mean ± SEM, $n = 3$). Unstimulated cells served as control and were set as 1. Values were referred to *GAPDH* as internal control. $^{*}p < 0.05$. **c** Western blot analysis of cellular lysates derived from control and tdnNrf2-transfected HuH7.5 cells and control and Nrf2-specific siRNA-transfected HepG2 cells using IRβ-specific antiserum. Cells were stimulated with tBHQ or left untreated. A rabbit-derived γ-GCSc-specific and a mouse-derived NQO1-specific antiserum served for detection of Nrf2-dependent marker proteins. Detection of β-actin served as loading control. **d** rtPCR of *IR*-specific transcripts in HuH7.5 cells transfected with control (pUC), constitutively active Nrf2 (caNrf2) and transdominant negative Nrf2 mutant (tdnNrf2) (mean ± SEM, $n = 2$). Control transfected cells served as control and were set as 1. Values were referred to *GAPDH* as internal control. Successful transfection with Nrf2 mutant was confirmed by increased or reduced expression of classical Nrf2 target gene GPx1 (not shown). **e** Western blot analysis of cellular lysates derived from control and tdnNrf2 transfected HepG2.2.15 cells using IRβ-specific antiserum. A rabbit-derived γ-GCSc-specific and a mouse-derived NQO1-specific antiserum served for detection of Nrf2-dependent marker proteins. Detection of β-actin served as loading control. **f** Immunohistochemical staining of NQO1 in liver sections from WT and HBV transgenic mice (magnification ×400). HBV expressing cells were visualized using a goat-derived SHBs-specific antiserum. For detection of NQO1, a rabbit-derived antibody was used. *Scale bar* represents 50 μm. **g** Immunohistochemical staining of liver sections from HBV transgenic wild type (HBV WT) and HBV transgenic Nrf2 knock-out (HBVΔNrf2$^{-/-}$) mice (magnification ×400). HBV expressing cells were visualized using a goat-derived SHBs-specific antiserum. For detection of IRβ, a rabbit-derived antibody was used. *Scale bar* represents 50 μm

Activation of Nrf2 induces insulin receptor expression

Recent reports described a tight crosstalk between Nrf2 and IR-dependent signaling [13]. As HBV activates Nrf2 [23], it was analyzed whether HBV-dependent activation of Nrf2 could contribute to the increased expression of IR in HBV replicating cells. Sequence analysis of the promoter of IR predicted the existence of two putative AREs which serve as target sequences for Nrf2 binding (Fig. 3a).

To study the impact of Nrf2 on the expression of the IR, Huh7.5 cells were treated with tBHQ. tBHQ is a widely used inducer of Nrf2 activity by triggering ROI production [42]. The amount of IR-specific transcripts before and after treatment was quantified by rtPCR. Quantification of GCLC-specific transcripts, an established Nrf2-dependent marker gene, served as control. rtPCR analysis shows that the expression of the IR gene is induced by tBHQ (Fig. 3b). Co-expression of a transdominant negative mutant of Nrf2 (tdnNrf2) Nrf2 abolishes this activation, indicating that Nrf2 indeed mediates the tBHQ-dependent activation of the IR gene (Fig. 3b). Western blot analyses of cellular lysates derived from tBHQ-treated, pUC18-transfected Huh7.5 cells using an IRβ-specific antibody confirmed the tBHQ-dependent induction of IRβ expression (Fig. 3c). Transfection of an expression vector encoding for tdnNrf2 or a specific siRNA-mediated knockdown abolishes the tBHQ-specific induction (Fig. 3c). Detection of the Nrf2-specific marker proteins NQO1 and γ-GCSc served as control.

To directly demonstrate the relevance of Nrf2 for the expression of IR, Huh7.5 cells were transfected with a constitutive active mutant of Nrf2 (caNrf2). The subsequent rtPCR analysis shows that expression of caNrf2 induces the expression of IR (Fig. 3d).

To investigate whether indeed the HBV-dependent induction of Nrf2 confers to the elevated amount of IR in HBV expressing cells, HepG2.2.15 cells were either transfected with ptdnNrf2 or with pUC18 as control. The Western blot analysis of the corresponding cellular lysates shows that expression of tdnNrf2 leads to a significant decrease in the amount of IR (Fig. 3e).

Immunofluorescence microscopy of liver samples derived from HBV transgenic mice using a NQO1-specific antibody confirms the activation of Nrf2 in the HBV transgenic mice (Fig. 3f). Immunofluorescence microscopy of liver samples derived from HBV transgenic Nrf2 knock-out mice shows that in these mice no increased amount of IR is detectable (Fig. 3g). This confirms the relevance of Nrf2 for the HBV-dependent induction of IR expression.

Taken together, these data indicate that HBV via activation of Nrf2 induces the expression of IR.

Intracellular retention of the insulin receptor in HBV expressing cells

The data described above demonstrate that in HBV transgenic mice liver regeneration is diminished. In accordance with this, an impaired insulin signaling is found. However, this is obviously not due to decreased amounts of IR. Therefore, it was investigated whether HBV expression affects insulin binding. To address this question, primary hepatocytes were isolated from HBV transgenic mice and the corresponding WT control mice and incubated with FITC-labeled insulin. Quantification of specifically surface-bound FITC-insulin reveals significantly reduced insulin binding in hepatocytes derived from HBV transgenic mice (Fig. 4a).

For a more detailed analysis, the HBV expressing stable cell lines HepG2.2.15 and HepAD38 were used in comparison to HepG2 cells. Determination of the FITC-insulin binding confirms decreased insulin binding of HBV expressing cells (Fig. 4b). Flow cytometry analyses using an IR-specific antiserum reveals that this is due to a

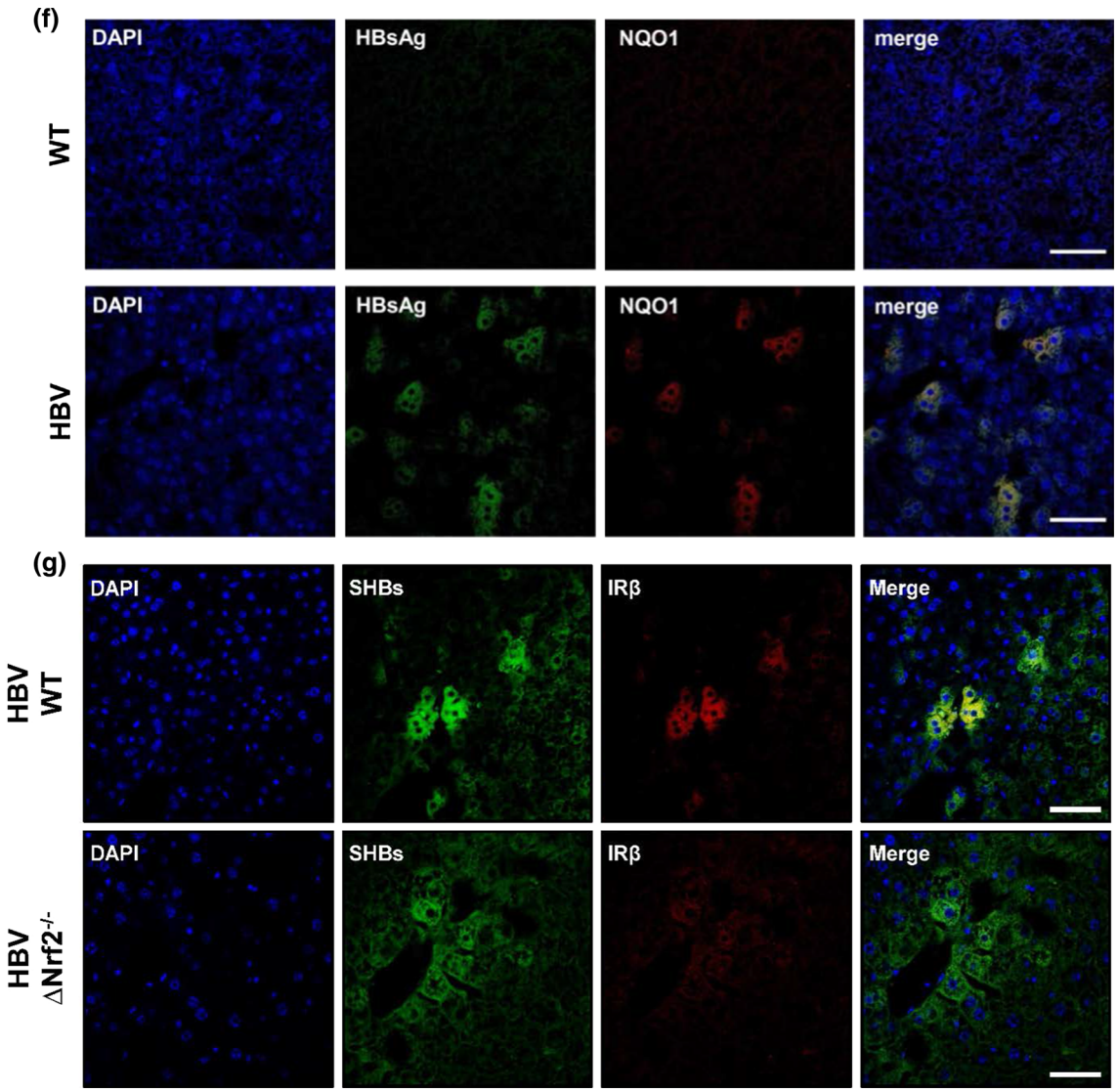

Fig. 3 continued

diminished amount of IR on the surface of HBV expressing cells (Fig. 4c). Western blot analyses of plasma membrane fractions isolated from HepG2.2.15 and HepG2 cells confirms that in the plasma membrane fraction derived from HBV expressing cells a reduced amount of IR is found, as compared to HepG2 cells (Fig. 4d). Further analyses showed that in contrast to IR, the amount of insulin like growth factor I receptor β (IGF-IRβ) is not reduced in the plasma membrane of HBV expressing cells (Fig. 4e).

The data described above demonstrate that in HBV-positive cells the total amount of IR is elevated, while the number of IR on the surface is decreased. Based on this, it was hypothesized that in HBV expressing cells the IR is intracellularly retained. To investigate this, subcellular fractionation of lysates derived from HepG2 and HepAD38 cells were performed by iodixanol density gradient centrifugation for separation of Golgi membranes from ER membranes. Determination of enzymatic galactosyltransferase (galT) activity as Golgi marker and detection of protein disulfide isomerase (PDI) by Western blot as ER marker was performed to control the isolation of the different subcellular compartments. Western blot analyses of the fractions isolated from the density gradient reveals that in HepG2 cells in the fractions corresponding to ER and Golgi membranes significant amounts of IR are detectable. In case of HBV expressing cells (HepAD38), the IR is enriched in the ER and the ratio between ER-localized to Golgi-localized IR is significantly elevated as compared to the HepG2 cells (Fig. 4f). This indicates that in HBV expressing cells the IR is retained in the ER and a significant smaller fraction enters the Golgi complex.

Taken together, these data demonstrate that HBV expressing cells exhibit a reduced binding capacity for insulin due to intracellular retention of the receptor.

Elevated amounts of α-taxilin lead to intracellular retention of the insulin receptor

In HBV expressing cells, the amount of α-taxilin is elevated, as described recently [43]. α-Taxilin acts as an adapter between the ESCRT machinery and the HBV surface proteins [43]. Moreover, α-taxilin has the capacity to bind to members of the syntaxin family (syntaxin 1, 2 and 4) [44]. As α-taxilin exclusively binds to free syntaxin that is not part of the SNARE complex, it exerts a negative effect on SNARE complex formation and therefore, vesicular trafficking [45]. In light of this, it was investigated whether elevated levels of α-taxilin in HBV expressing cells could be causative for the observed intracellular retention of IR. Immunofluorescence analysis of liver samples derived from transgenic mice reveal significant higher amounts of α-taxilin in HBV transgenic mice as compared to the corresponding WT animals (Fig. 5a). In accordance with this, expression analysis by rtPCR as well as western blot analysis of HBV-infected primary human hepatocytes (PHH) reveals elevated amounts of α-taxilin-specific transcripts and protein as compared to uninfected controls (Fig. 5b).

For a more detailed analysis, HuH7.5 cells were transfected with an expression vector encoding for a fusion protein of mcherry and α-taxilin. Transfection with an mcherry-encoding vector served as control. These cells were incubated with FITC-insulin and analyzed by flow cytometry. Gating of the red fluorescent cells reveals that in case of the mcherry-taxilin expressing cells, a significant lower binding of FITC-insulin is observed as compared to the mcherry-expressing control cells (Fig. 5c).

These data indicate that HBV via elevated levels of α-taxilin impairs the transport of IR to the plasma membrane.

Reduced insulin responsiveness in HBV expressing cells

The data described above indicate that in HBV expressing cells the transport of IR to the plasma membrane is impaired. The resulting question was whether this indeed leads to an impaired induction of insulin receptor signaling. To address this, HBV expressing HepAD38 cells and HepG2 control cells were stimulated with insulin and the formation of tyrosine-phosphorylated IRβ subunit was analyzed by Western blot and phospho-IRβ-specific ELISA. The Western blot as well as the ELISA analysis reveal a significant lower tyrosine phosphorylation of IR upon insulin stimulation in HBV-positive cells as compared to the control (Fig. 6a, b). In accordance with the reduced insulin responsiveness, the glucose concentration in the supernatant of insulin-stimulated HepG2 cells is significantly diminished in contrast to the HBV expressing HepAD38 cells. Here, insulin stimulation causes no significant reduction in the glucose concentration of the medium (Fig. 6c). Expression analysis of the insulin-dependent marker gene glucokinase (GCK) reveals an insulin-dependent stimulation in HepG2 cells, while GCK expression in case of insulin-stimulated HepG2.2.15 cells remains almost unaffected (Fig. 6d). Regarding the basal expression of the insulin-dependent glucose transporter 4 (GLUT4), a significant lower expression was found for HBV expressing cell lines HepAD38 and HepG2.2.15 as compared to the HepG2 control cells (Fig. 6e).

This reduced insulin responsiveness is reflected by elevated glucose levels in the sera of HBV transgenic mice in comparison to the corresponding sera from WT mice (Fig. 6f).

Taken together, these data demonstrate that in HBV expressing cells the number of IR on the plasma membrane is reduced leading to an impaired responsiveness to insulin.

Discussion

Chronic HBV infection is frequently associated with the development of pathological changes of the liver like fibrosis, cirrhosis or HCC [7]. Chronic active hepatitis B is characterized by an insufficient elimination of infected hepatocytes by the cellular immune response leading to an equilibrium between partial elimination of infected hepatocytes, regeneration and reinfection [8]. In case of a persistent infection, fibroblasts and connective tissue can replace more and more functional hepatocytes that can reflect an impaired liver regeneration [13, 46].

In case of hepatitis C virus (HCV), there is evidence that HCV leads to elevated ROI levels. Impaired activation of the cytoprotective transcription factor Nrf2 in HCV-positive cells [47] might contribute to the elevated level of ROI in case of chronic HCV infection, leading to JNK activation and subsequent inactivation of insulin signaling that plays an essential role for the control of liver regeneration. In light of the observed relevance of Nrf2 for the expression of the insulin receptor, the impaired activation of Nrf2 in HCV-replicating cells could lead to a reduced expression of the insulin receptor.

While it is well established that chronic HBV infection is frequently associated with severe pathological changes of the liver, the direct impact of HBV on processes controlling liver regeneration is not fully understood. In this study, we observed that in HBV transgenic mice after CCl_4-induced liver damage the regeneration in HBV

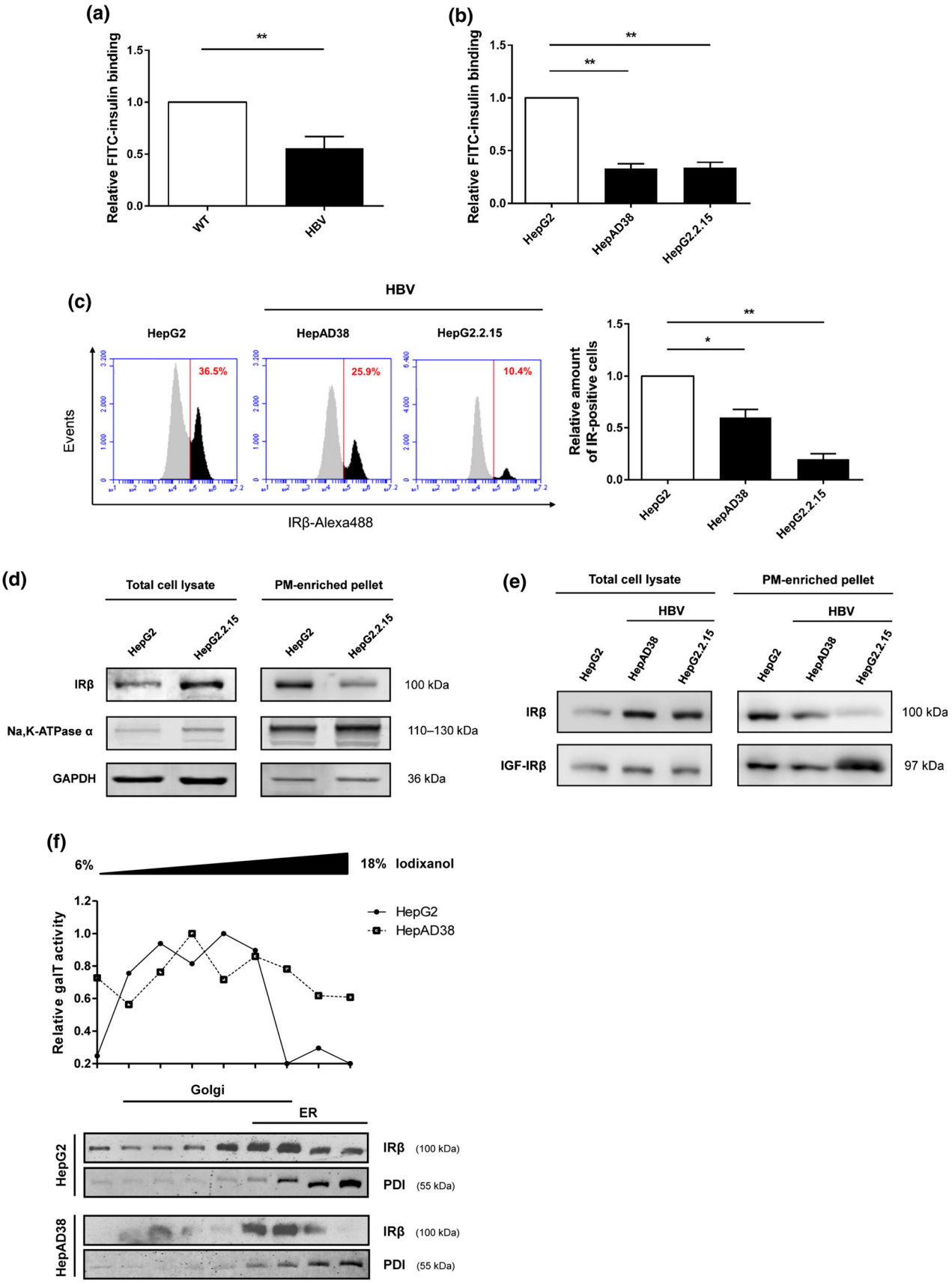
(a)
Relative FITC-insulin binding
1.5
1.0
0.5
0.0
**
WT
HBV
(b)
Relative FITC-insulin binding
**
**
HepG2
HepAD38
HepG2.2.15
(c)
HBV
HepG2
HepAD38
HepG2.2.15
36.5%
25.9%
10.4%
Events
IRβ-Alexa488
Relative amount of IR-positive cells
**
*
(d)
Total cell lysate
PM-enriched pellet
HepG2
HepG2.2.15
IRβ
Na,K-ATPase α
GAPDH
100 kDa
110–130 kDa
36 kDa
(e)
Total cell lysate
PM-enriched pellet
HBV
HepG2
HepAD38
HepG2.2.15
IRβ
IGF-IRβ
100 kDa
97 kDa
(f)
6%
18% Iodixanol
Relative galT activity
HepG2
HepAD38
Golgi
ER
HepG2
HepAD38
IRβ (100 kDa)
PDI (55 kDa)

◀**Fig. 4** Reduced amounts of surface-bound insulin receptor lead to decreased insulin binding in HBV expressing cells. **a** Primary hepatocytes from WT and HBV transgenic mice were incubated with FITC-labeled insulin and relative FITC-fluorescence was measured in a microplate fluorescent plate reader ($n = 3$, mean ± SEM). WT mouse cells were set as 1. $^{**}p < 0.01$. **b** HepG2, HepAD38 and HepG2.2.15 cells were incubated with FITC-labeled insulin and relative FITC-fluorescence was measured in a microplate fluorescent plate reader ($n = 3$, mean ± SEM). HepG2 cells were set as 1. $^{**}p < 0.01$. **c** Non-permeabilized HepG2, HepAD38 and HepG2.2.15 cells were incubated with a rabbit-derived IRβ-specific antiserum and a donkey-derived Alexa488-coupled anti-rabbit secondary antibody. Viable cells were gated by flow cytometry and percentage of cells expressing insulin receptor on the cell surface were analyzed. One representative histogram is shown of three independent experiments. As a control, the cells were only incubated with the donkey-derived Alexa488-coupled secondary antibody (*gray-shaded peaks*) to determine background fluorescence originating from the cells. Summary of flow cytometry analysis ($n = 3$, mean ± SEM) is shown in the diagram. HepG2 cells were set as 1. $^{*}p < 0.05$, $^{**}p < 0.01$. **d** Western blot analysis of total cellular lysates and plasma membrane-enriched fractions derived from HepG2 and HepG2.2.15 cells using rabbit-derived IRβ-specific antiserum. Enrichment of plasma membrane was confirmed by detection of membrane-localized Na^+/K^+-ATPase α and depletion of cytosolic GAPDH. Residual amounts of GAPDH after enrichment represent membrane-associated GAPDH. Similar results were obtained for stably HBV expressing HepAD38 cells. **e** Western blot analysis of total cellular lysates and plasma membrane-enriched fractions derived from HepG2, HepAD38 and HepG2.2.15 cells using rabbit-derived IRβ- and IGFRβ-specific antisera. **f** Cellular lysates from HepG2 and HepAD38 cells were used for subcellular fractionation by iodixanol density gradient centrifugation. Fractions were collected from top to bottom and analyzed by galactosyltransferase (galT) activity assay (*upper panel*) for the presence of Golgi membranes and the presence of IRβ and ER-resident protein PDI by western blot using rabbit-derived IRβ- and mouse-derived PDI-specific antisera (*lower panel*). Comparable results were obtained for HepG2.2.15 cells using a mouse-derived antiserum against calnexin as marker for ER in the western blot. The range of iodixanol concentration of the analyzed fractions is indicated *above* the graph in **a**. The fractions analyzed in the galT assay above the blot correspond to the fractions analyzed by western blot

transgenic mice is impaired (Fig. 1a, b). In case of long-term application, increased formation of collagen and α-SMA was detected in the liver samples derived from HBV transgenic mice as compared to the CCl_4-treated HBV-negative control mice (Fig. 1d, e). This is in contrast to a recent report by Tian et al. [48]. They report that HBV seems to have no impact on liver regeneration. However, the study by Tian et al. is based on partial hepatectomy (PHx), and liver regeneration was assessed based on the determination of liver weight gain 10 days after PHx that might be not suitable to resolve moderate changes in the proliferative potential. In addition, PCNA staining was performed 72 h after PHx. At this time point, the proliferation rate of murine hepatocytes is already decreasing in the WT mice and upregulated in HBV transgenic mice due to the delayed onset of the repair process [49] (Fig. 1b). In contrast to this, we analyzed hepatocyte proliferation over the course of 7 days after CCl_4-induced damage. Especially 2 days after the CCl_4 treatment hepatocyte proliferation peaks, which are the differences between WT and HBV transgenic mice are more pronounced. There are several reports describing an inhibitory effect of HBV on hepatocyte proliferation [50, 51], primarily triggered by the action of the regulatory proteins HBx and LHBs (PreS2-activator) [52–56]. In addition, there is a previous report about a direct inhibitory interference of HBV with insulin signaling where HBx was described to promote degradation of IRS1 and to induce SOCS3 [57]. Moreover, there is evidence for a general inhibitory effect of HBV on cell cycle progression. HBV triggers an induction of p21cip1/waf1 expression that is reflected by a reduction of cyclin A associated cdk2 activity and an increase of cyclin E associated cdk2 activity. This means that HBV producing cells progress through the G1 phase (triggered by the increased cyclin E associated cdk2 activity). Further progression through the cell cycle, the entry in the S phase, is blocked since the activity of cyclin A associated cdk2 activity is reduced [50].

In our study, we observe a diminished activation of insulin receptor signaling (Figs. 1c, 6a, b) and describe a novel mechanism that contributes to the uncoupling of HBV expressing hepatocytes from the insulin receptor signaling pathway (Fig. 7). Although due to the activation of Nrf2, the expression and amount of IR is increased in HBV expressing cells (Fig. 2), the receptor is not targeted to the plasma membrane but it is intracellularly retained (Fig. 4f). This leads to diminished insulin binding and in accordance with this to a reduced sensitivity of these cells to insulin signaling (Figs. 4a, b, 6d).

We revealed elevated amounts of α-taxilin as a causative factor for the intracellular retention of IR in HBV expressing cells (Fig. 5c). We have previously described that in HBV expressing cells the amount of α-taxilin is increased [43]. In this study, we confirm this for HBV transgenic mice and for HBV-infected PHH (Fig. 5a, b). In contrast to the expression of IR, the α-taxilin promoter harbors no ARE sites and in accordance to this the expression of α-taxilin does not depend on Nrf2 (unpublished results S.B.). α-Taxilin was observed to bind on the one hand to LHBs, and on the other hand by a YAEL motive, that represents a classic late domain, to the ESCRT component tsg101 [43]. α-Taxilin has been found to bind to the members of the syntaxin family (syntaxin 1, 2 and 4) [44]. However, α-taxilin exclusively binds to free syntaxin that is not part of the SNARE complex [45]. Therefore, α-taxilin acts as a negative regulator of the SNARE complex formation by withdrawal of free syntaxin required for incorporation in forming the SNARE complexes and thereby impairing vesicular trafficking. Flow cytometry analysis of mcherry-taxilin over-expressing cells revealed that in α-taxilin overproducing cells the number of insulin

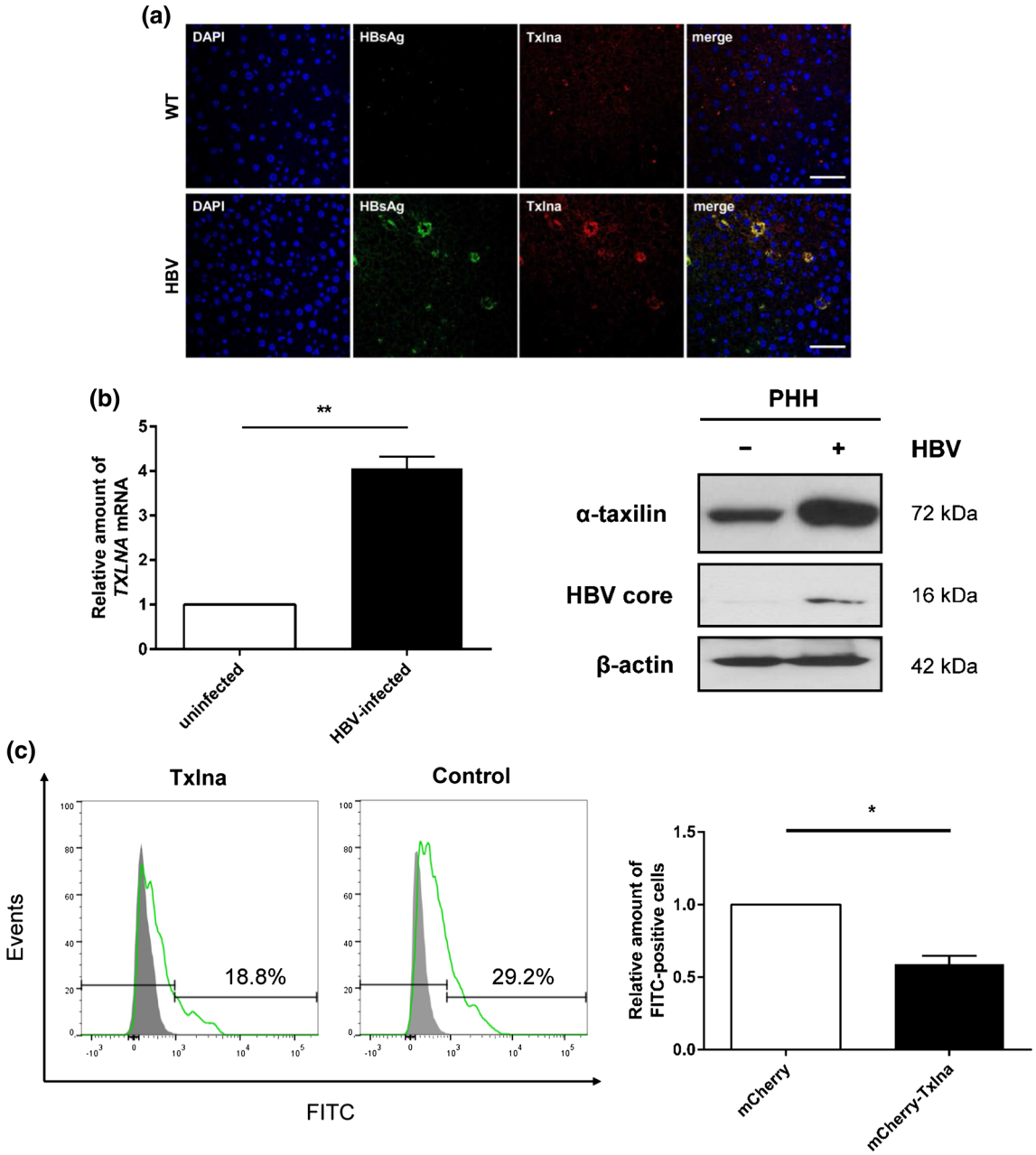

Fig. 5 Elevated amounts of α-taxilin in HBV expressing cells contribute to insulin receptor retention. **a** Immunohistochemical staining of α-taxilin (Txlna) in liver sections derived from WT and HBV transgenic mice (magnification ×200). HBV expressing cells were visualized using a goat-derived SHBs-specific antiserum. For detection of Txlna, a rabbit-derived antibody was used. Scale bar represents 50 µm. **b** rtPCR of *TXLNA*-specific transcripts in HBV-infected (MOI = 5) primary human hepatocytes (PHH) and uninfected controls ($n = 3$, mean ± SEM) referred to *GAPDH* as internal control. Uninfected cells were set as 1. $^{**}p < 0.01$. The western blot shows the amount of α-taxilin in cellular lysates derived from HBV-infected and uninfected PHH using a rabbit-derived α-taxilin-specific antiserum and for detection of HBV core protein a mouse-derived HBV core-specific antiserum. Detection of β-actin served as loading control. **c** HuH7.5 cells were either transfected with a plasmid encoding an mCherry-tagged α-taxilin fusion protein or mCherry alone (control) and were then incubated with 100 nM FITC-insulin. mCherry-Txlna or mCherry-expressing cells were gated by flow cytometry and analyzed for FITC-fluorescence. Gray-shaded peaks represent background fluorescence originating from cells that were not incubated with FITC-insulin. Representative histogram shows percentage of FITC-insulin-positive cells from mCherry-Txlna or mCherry-expressing control cells. Summary of flow cytometry analysis ($n = 4$, mean ± SEM) is shown in the diagram. Control cells were set as 1. $^{*}p < 0.05$

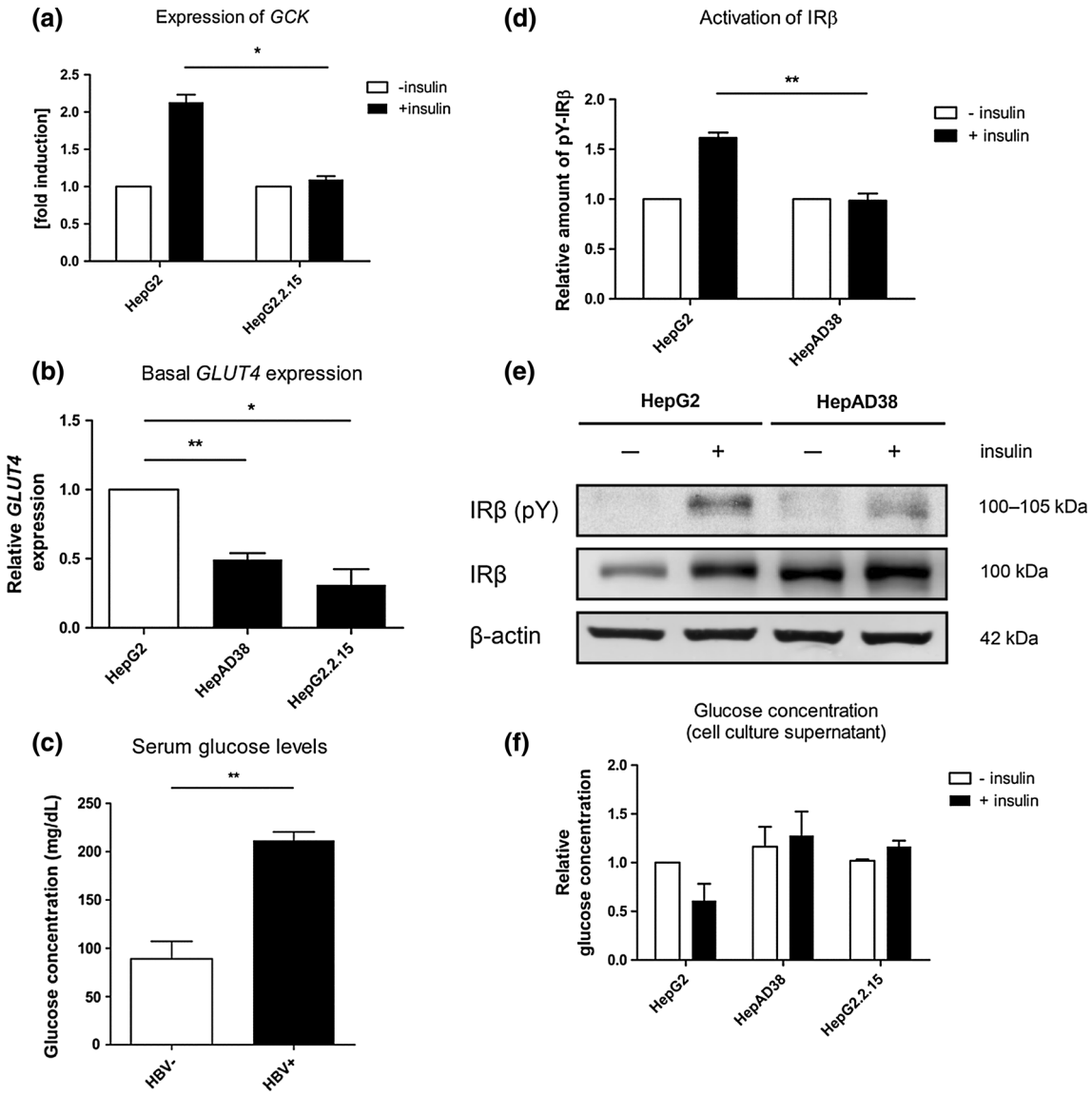

Fig. 6 Reduced insulin responsiveness in HBV expressing cells. **a**, **b** Activation of IRβ by tyrosine phosphorylation (pY) was determined by phospho-IRβ-specific ELISA (**a**) and western blot (**b**) of cellular lysates of HepG2 and HepAD38 with and without addition of 100 nM insulin for 20 min (ELISA) or 5 min (western blot) using a rabbit-derived phospho-IRβ-specific antiserum. Total amount of IRβ was determined by western blot using a rabbit-derived IRβ-specific antiserum. Detection of β-actin served as loading control. Unstimulated cells in **a** were set as 1. $^{**}p < 0.01$. **c** Glucose concentration was measured in the cell culture supernatant before and after insulin stimulation for 12 h with 100 nM insulin. Experiment was performed in duplicate. Unstimulated HepG2 cells were set as 1. **d** rtPCR of *GCK*-specific transcripts in HepG2 and HepG2.2.15 cells before and after stimulation for 2–4 h with 100 nM insulin ($n = 3$, mean ± SEM). Values were referred to *RPL27* as internal control. Unstimulated cells were set as 1. $^{*}p < 0.05$. **e** rtPCR of *GLUT4*-specific transcripts in HepG2, HepAD38 and HepG2.2.15 cells ($n = 5$, mean ± SEM). Values were referred to *RPL27* as internal control. HepG2 were set as 1. $^{*}p < 0.05$, $^{**}p < 0.01$. **f** Serum glucose concentration of 2–6 month old HBV-negative (HBV−) and HBV transgenic (HBV+) mice ($n = 3$, two males and one female per group, mean ± SEM). $^{**}p < 0.01$

receptors on the surface and thereby insulin binding capacity is reduced (Fig. 5c). Further experiments revealed that the targeting of IGF-IR to the plasma membrane is not affected by α-taxilin overexpression (Fig. 4e).

Functional experiments revealed that HBV expressing hepatocytes indeed are less sensitive to insulin stimulation (Fig. 4a, b). In accordance with this, an elevated glucose level is found in the serum of HBV transgenic mice (Fig. 6f). In light of this, the question arises "whether HBV patients develop type 2 diabetes?". Indeed, there are conflicting data about a potential correlation between chronic HBV and development of type 2 diabetes [58, 59]. However, it has to be considered that an elevated glucose level does not automatically lead to glucose levels found in

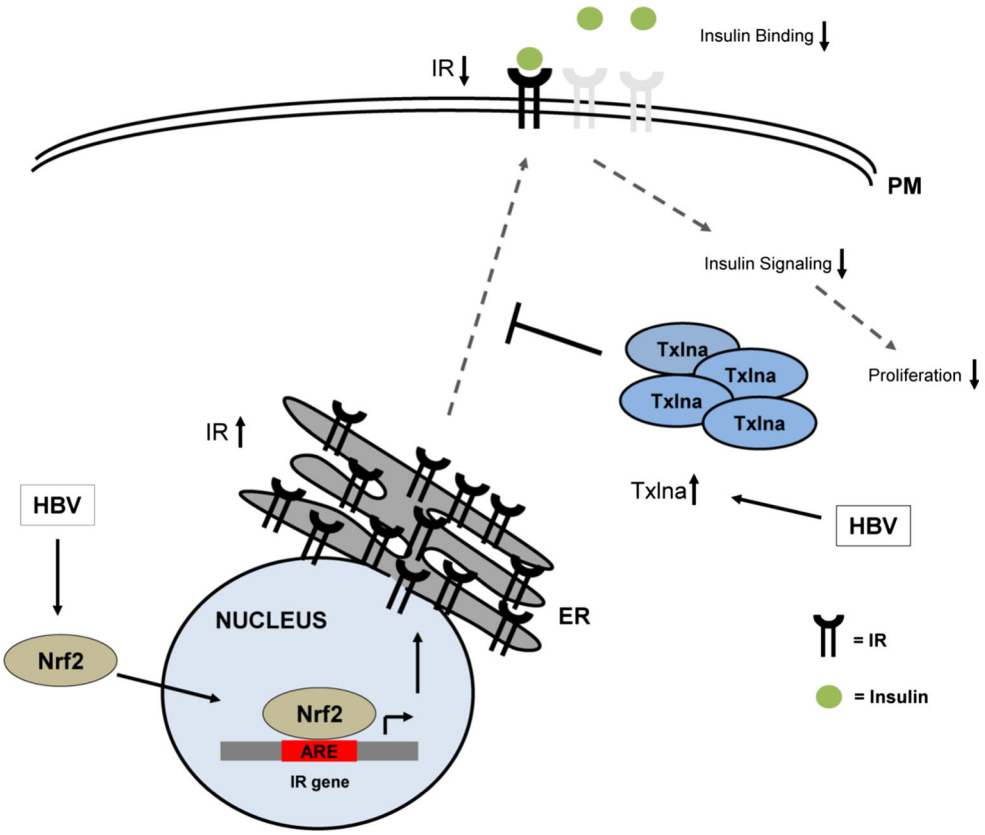

Fig. 7 Schematic representation of HBV-induced insulin receptor retention. HBV induces activation of Nrf2 which translocates to the nucleus and activates ARE-mediated expression of the insulin receptor (*IR*). In parallel, HBV also induces increased amounts of α-taxilin (Txlna) which prevent insulin receptor translocation to the plasma membrane (PM) resulting in accumulation of the insulin receptor at the endoplasmic reticulum (ER). Reduced amounts of the insulin receptor at the plasma membrane attenuate insulin binding and lead to inhibition of insulin receptor signaling and retardation of hepatocyte proliferation

diabetic patients. Moreover, in case of the mice, the liver plays a more essential role for the glucose homeostasis as compared to humans where skeletal muscle, adipose tissue and kidney are more relevant for the control of glucose levels [60–63]. However, the elevated serum glucose levels found in the HBV transgenic mice support the observation that insulin receptor signaling is impaired in HBV expressing cells.

In addition to the interference with the insulin signaling, the HBV-dependent induction of Nrf2 can lead to a situation as observed for transgenic mice that express constitutive active Nrf2 (caNrf2). In these mice, liver regeneration is impaired due to delayed hepatocyte proliferation and enhanced apoptosis as the expression of the cyclin-dependent kinase inhibitor p15 and Bcl2l11 (Bim) is upregulated [22].

Taken together, this study describes a so far unprecedented pathomechanism in HBV expressing hepatocytes where the insulin receptor is intracellularly retained, preventing compensatory liver regeneration that finally could foster chronic liver damage and liver disease progression.

Acknowledgments We thank Marion Wingerter for the preparation of consecutive liver sections and histological stainings. We feel indebted to Dr. Meike Gratz, Dr. Kiyoshi Himmelsbach, Dr. Daniela Ploen, Andrea Henkes and Alena Zindel for constant helpfulness and Dagmar Fecht-Schwarz for her critical reading of the manuscript.

Compliance with ethical standards

Conflict of interest The authors declare that they have no conflicts of interest with the contents of this article.

Funding information This work was supported by grants of the Wilhelm-Sander-Stiftung, Munich, and from the DZIF to EH. The funders had no role in study design, data collection and interpretation, or the decision to submit the work for publication.

References

1. Schädler S, Hildt E (2009) HBV life cycle: entry and morphogenesis. Viruses 1:185–209. doi:10.3390/v1020185
2. Liang TJ, Block TM, McMahon BJ, Ghany MG, Urban S, Guo J et al (2015) Present and future therapies of hepatitis B: from discovery to cure. Hepatology 62:1893–1908. doi:10.1002/hep.28025
3. Arzumanyan A, Reis H, Feitelson MA (2013) Pathogenic mechanisms in HBV- and HCV-associated hepatocellular carcinoma. Nat Rev Cancer 13:123–135. doi:10.1038/nrc3449
4. Lupberger J, Hildt E (2007) Hepatitis B virus-induced oncogenesis. World J Gastroenterol 13:74. doi:10.3748/wjg.v13.i1.74
5. Dhanasekaran R, Limaye A, Cabrera R (2012) Hepatocellular carcinoma: current trends in worldwide epidemiology, risk factors, diagnosis, and therapeutics. Hepat Med 4:19–37. doi:10.2147/HMER.S16316
6. Thimme R, Wieland S, Steiger C, Ghrayeb J, Reimann KA, Purcell RH et al (2003) $CD8^+$ T cells mediate viral clearance and disease pathogenesis during acute hepatitis B virus infection. J Virol 77:68–76. doi:10.1128/JVI.77.1.68-76.2003

7. Guidotti LG, Chisari FV (2006) Immunobiology and pathogenesis of viral hepatitis. Annu Rev Pathol 1:23–61. doi:10.1146/annurev.pathol.1.110304.100230
8. Chisari FV, Isogawa M, Wieland SF (2010) Pathogenesis of hepatitis B virus infection. Pathol Biol 58:258–266. doi:10.1016/j.patbio.2009.11.001
9. Fausto N, Campbell JS, Riehle KJ (2006) Liver regeneration. Hepatology 43:S45–S53. doi:10.1002/hep.20969
10. Xu R, Zhang Z, Wang F (2012) Liver fibrosis: mechanisms of immune-mediated liver injury. Cell Mol Immunol 9:296–301. doi:10.1038/cmi.2011.53
11. Yamada T, Yamamoto M, Ozawa K, Honjo I (1977) Insulin requirements for hepatic regeneration following hepatectomy. Ann Surg 185:35–42
12. Beyer TA, Werner S (2008) The cytoprotective Nrf2 transcription factor controls insulin receptor signaling in the regenerating liver. Cell Cycle 7:874–878. doi:10.4161/cc.7.7.5617
13. Beyer TA, Xu W, Teupser D, auf dem Keller U, Bugnon P, Hildt E et al (2008) Impaired liver regeneration in Nrf2 knockout mice: role of ROS-mediated insulin/IGF-1 resistance. EMBO J 27:212–223. doi:10.1038/sj.emboj.7601950
14. Böhm F, Köhler UA, Speicher T, Werner S (2010) Regulation of liver regeneration by growth factors and cytokines. EMBO Mol Med 2:294–305. doi:10.1002/emmm.201000085
15. Ozawa K, Ida T, Yamada T, Honjo I (1976) Significance of glucose tolerance as prognostic sign in hepatectomized patients. Am J Surg 131:541–546
16. Itoh K, Chiba T, Takahashi S, Ishii T, Igarashi K, Katoh Y et al (1997) An Nrf2/Small Maf heterodimer mediates the induction of phase II detoxifying enzyme genes through antioxidant response elements. Biochem Biophys Res Commun 236:313–322. doi:10.1006/bbrc.1997.6943
17. Aleksunes LM, Manautou JE (2007) Emerging role of Nrf2 in protecting against hepatic and gastrointestinal disease. Toxicol Pathol 35:459–473. doi:10.1080/01926230701311344
18. Kensler TW, Wakabayashi N, Biswal S (2007) Cell survival responses to environmental stresses via the Keap1-Nrf2-ARE pathway. Annu Rev Pharmacol Toxicol 47:89–116. doi:10.1146/annurev.pharmtox.46.120604.141046
19. Jaiswal AK (2004) Nrf2 signaling in coordinated activation of antioxidant gene expression. Free Radic Biol Med 36:1199–1207. doi:10.1016/j.freeradbiomed.2004.02.074
20. Ross D, Kepa JK, Winski SL, Beall HD, Anwar A, Siegel D (2000) NAD(P)H: quinone oxidoreductase 1 (NQO1): chemoprotection, bioactivation, gene regulation and genetic polymorphisms. Chem Biol Interact 129:77–97. doi:10.1016/S0009-2797(00)00199-X
21. Wasserman WW, Fahl WE (1997) Functional antioxidant responsive elements. Proc Natl Acad Sci USA 94:5361–5366
22. Köhler UA, Kurinna S, Schwitter D, Marti A, Schäfer M, Hellerbrand C et al (2014) Activated Nrf2 impairs liver regeneration in mice by activation of genes involved in cell-cycle control and apoptosis. Hepatology 60:670–678. doi:10.1002/hep.26964
23. Schädler S, Krause J, Himmelsbach K, Carvajal-Yepes M, Lieder F, Klingel K et al (2010) Hepatitis B virus induces expression of antioxidant response element-regulated genes by activation of Nrf2. J Biol Chem 285:41074–41086. doi:10.1074/jbc.M110.145862
24. Tachtatzis PM, Marshall A, Arvinthan A, Aravinthan A, Verma S, Penrhyn-Lowe S et al (2015) Chronic hepatitis B virus infection: the relation between hepatitis B antigen expression, telomere length, senescence, inflammation and fibrosis. PLoS One 10:e0127511. doi:10.1371/journal.pone.0127511
25. Guidotti LG, Matzke B, Schaller H, Chisari FV (1995) High-level hepatitis B virus replication in transgenic mice. J Virol 69:6158–6169
26. Chan K, Kan YW (1999) Nrf2 is essential for protection against acute pulmonary injury in mice. Proc Natl Acad Sci USA 96:12731–12736
27. Mederacke I, Dapito DH, Affò S, Uchinami H, Schwabe RF (2015) High-yield and high-purity isolation of hepatic stellate cells from normal and fibrotic mouse livers. Nat Protoc 10:305–315. doi:10.1038/nprot.2015.017
28. Ladner SK, Otto MJ, Barker CS, Zaifert K, Wang GH, Guo JT et al (1997) Inducible expression of human hepatitis B virus (HBV) in stably transfected hepatoblastoma cells: a novel system for screening potential inhibitors of HBV replication. Antimicrob Agents Chemother 41:1715–1720
29. Sells MA, Chen ML, Acs G (1987) Production of hepatitis B virus particles in Hep G2 cells transfected with cloned hepatitis B virus DNA. Proc Natl Acad Sci USA 84:1005–1009
30. Ehrhardt C, Schmolke M, Matzke A, Knoblauch A, Will C, Wixler V et al (2006) Polyethylenimine, a cost-effective transfection reagent. Signal Transduct 6:179–184. doi:10.1002/sita.200500073
31. Dayoub R, Thasler WE, Bosserhoff AK, Singer T, Jauch K, Schlitt HJ et al (2006) Regulation of polyamine synthesis in human hepatocytes by hepatotrophic factor augmenter of liver regeneration. Biochem Biophys Res Commun 345:181–187. doi:10.1016/j.bbrc.2006.04.040
32. Lupberger J, Mund A, Kock J, Hildt E (2006) Cultivation of HepG2.2.15 on Cytodex-3: higher yield of hepatitis B virus and less subviral particles compared to conventional culture methods. J Hepatol 45:547–552. doi:10.1016/j.jhep.2006.05.012
33. auf dem Keller U, Huber M, Beyer TA, Kümin A, Siemes C, Braun S et al (2006) Nrf transcription factors in keratinocytes are essential for skin tumor prevention but not for wound healing. Mol Cell Biol 26:3773–3784. doi:10.1128/MCB.26.10.3773-3784.2006
34. Laemmli UK (1970) Cleavage of structural proteins during the assembly of the head of bacteriophage T4. Nature 227:680–685. doi:10.1038/227680a0
35. Bürckstümmer T, Kriegs M, Lupberger J, Pauli EK, Schmittel S, Hildt E (2006) Raf-1 kinase associates with hepatitis C virus NS5A and regulates viral replication. FEBS Lett 580:575–580. doi:10.1016/j.febslet.2005.12.071
36. Heermann KH, Goldmann U, Schwartz W, Seyffarth T, Baumgarten H, Gerlich WH (1984) Large surface proteins of hepatitis B virus containing the pre-s sequence. J Virol 52:396–402
37. Ploen D, Hafirassou ML, Himmelsbach K, Schille SA, Biniossek ML, Baumert TF et al (2013) TIP47 is associated with the hepatitis C virus and its interaction with Rab9 is required for release of viral particles. Eur J Cell Biol 92:374–382. doi:10.1016/j.ejcb.2013.12.003
38. Junqueira LC, Bignolas G, Brentani RR (1979) Picrosirius staining plus polarization microscopy, a specific method for collagen detection in tissue sections. Histochem J 11:447–455
39. Puchtler H, Waldrop FS, Valentine LS (1973) Polarization microscopic studies of connective tissue stained with picro-sirius red FBA. Beitr Pathol 150:174–187
40. Procino G, Barbieri C, Carmosino M, Rizzo F, Valenti G, Svelto M (2010) Lovastatin-induced cholesterol depletion affects both apical sorting and endocytosis of aquaporin-2 in renal cells. Am J Physiol Renal Physiol 298:F266–F278. doi:10.1152/ajprenal.00359.2009
41. Deng C, Chen RR (2004) A pH-sensitive assay for galactosyltransferase. Anal Biochem 330:219–226. doi:10.1016/j.ab.2004.03.014
42. Imhoff BR, Hansen JM (2010) Tert-butylhydroquinone induces mitochondrial oxidative stress causing Nrf2 activation. Cell Biol Toxicol 26:541–551. doi:10.1007/s10565-010-9162-6

43. Hoffmann J, Boehm C, Himmelsbach K, Donnerhak C, Roettger H, Weiss TS et al (2013) Identification of α-taxilin as an essential factor for the life cycle of hepatitis B virus. J Hepatol 59:934–941. doi:10.1016/j.jhep.2013.06.020
44. Nogami S, Satoh S, Nakano M, Shimizu H, Fukushima H, Maruyama A et al (2003) Taxilin; a novel syntaxin-binding protein that is involved in Ca^{2+}-dependent exocytosis in neuroendocrine cells. Genes Cells 8:17–28. doi:10.1046/j.1365-2443.2003.00612.x
45. Nogami S, Satoh S, Nakano M, Terano A, Shirataki H (2003) Interaction of taxilin with syntaxin which does not form the SNARE complex. Biochem Biophys Res Commun 311:797–802. doi:10.1016/j.bbrc.2003.10.069
46. Diehl AM (2002) Liver regeneration. Front Biosci 7:e301–e314
47. Carvajal-Yepes M, Himmelsbach K, Schaedler S, Ploen D, Krause J, Ludwig L et al (2011) Hepatitis C virus impairs the induction of cytoprotective Nrf2 target genes by delocalization of small Maf proteins. J Biol Chem 286:8941–8951. doi:10.1074/jbc.M110.186684
48. Tian Y, Chen W, Kuo C, Ou JJ (2012) Viral-load-dependent effects of liver injury and regeneration on hepatitis B virus replication in mice. J Virol 86:9599–9605. doi:10.1128/JVI.01087-12
49. Taub R (2004) Liver regeneration: from myth to mechanism. Nat Rev Mol Cell Biol 5:836–847. doi:10.1038/nrm1489
50. Friedrich B, Wollersheim M, Brandenburg B, Foerste R, Will H, Hildt E (2005) Induction of anti-proliferative mechanisms in hepatitis B virus producing cells. J Hepatol 43:696–703. doi:10.1016/j.jhep.2005.02.026
51. Dong Z, Zhang J, Sun R, Wei H, Tian Z (2007) Impairment of liver regeneration correlates with activated hepatic NKT cells in HBV transgenic mice. Hepatology 45:1400–1412. doi:10.1002/hep.21597
52. Quétier I, Brezillon N, Duriez M, Massinet H, Giang E, Ahodantin J et al (2013) Hepatitis B virus HBx protein impairs liver regeneration through enhanced expression of IL-6 in transgenic mice. J Hepatol 59:285–291. doi:10.1016/j.jhep.2013.03.021
53. Park E, Park YK, Shin CY, Park SH, Ahn SH, Kim DH et al (2013) Hepatitis B virus inhibits liver regeneration via epigenetic regulation of urokinase-type plasminogen activator. Hepatology 58:762–776. doi:10.1002/hep.26379
54. Hodgson AJ, Keasler VV, Slagle BL (2008) Premature cell cycle entry induced by hepatitis B virus regulatory HBx protein during compensatory liver regeneration. Cancer Res 68:10341–10348. doi:10.1158/0008-5472.CAN-08-2695
55. Wu B, Li C, Chen H, Chang J, Jeng K, Chou C et al (2006) Blocking of G1/S transition and cell death in the regenerating liver of Hepatitis B virus X protein transgenic mice. Biochem Biophys Res Commun 340:916–928. doi:10.1016/j.bbrc.2005.12.089
56. Tralhao JG, Roudier J, Morosan S, Giannini C, Tu H, Goulenok C et al (2002) Paracrine in vivo inhibitory effects of hepatitis B virus X protein (HBx) on liver cell proliferation: an alternative mechanism of HBx-related pathogenesis. Proc Natl Acad Sci USA 99:6991–6996. doi:10.1073/pnas.092657699
57. Kim K, Kim KH, Cheong J (2010) Hepatitis B virus X protein impairs hepatic insulin signaling through degradation of IRS1 and induction of SOCS3. PLoS One 5:e8649. doi:10.1371/journal.pone.0008649
58. Zhang J, Shen Y, Cai H, Liu Y, Qin G (2015) Hepatitis B virus infection status and risk of type 2 diabetes mellitus: a meta-analysis. Hepatol Res. doi:10.1111/hepr.12481
59. Khalili M, Lombardero M, Chung RT, Terrault NA, Ghany MG, Kim WR et al (2015) Diabetes and prediabetes in patients with hepatitis B residing in North America. Hepatology 62:1364–1374. doi:10.1002/hep.28110
60. Mårin P, Rebuffé-Scrive M, Smith U, Björntorp P (1987) Glucose uptake in human adipose tissue. Metabolism 36:1154–1160
61. Cersosimo E, Garlick P, Ferretti J (1999) Insulin regulation of renal glucose metabolism in humans. Am J Physiol 276:E78–E84
62. Meyer C, Dostou JM, Welle SL, Gerich JE (2002) Role of human liver, kidney, and skeletal muscle in postprandial glucose homeostasis. Am J Physiol Endocrinol Metab 282:E419–E427. doi:10.1152/ajpendo.00032.2001
63. Marsenic O (2009) Glucose control by the kidney: an emerging target in diabetes. Am J Kidney Dis 53:875–883. doi:10.1053/j.ajkd.2008.12.031